

# Comparison Study on Single Nucleotide Transport Phenomena in Carbon Nanotubes

Yunjiao Wang, Zequn Wang, Liang Wang, Tianze Tong, Xiaoling Zhang, Shaoxi Fang, Wanyi Xie, Liyuan Liang, Bohua Yin, Jiahu Yuan,\* Jin Zhang,\* and Deqiang Wang\*



Cite This: *Nano Lett.* 2022, 22, 2147–2154



Read Online

ACCESS |

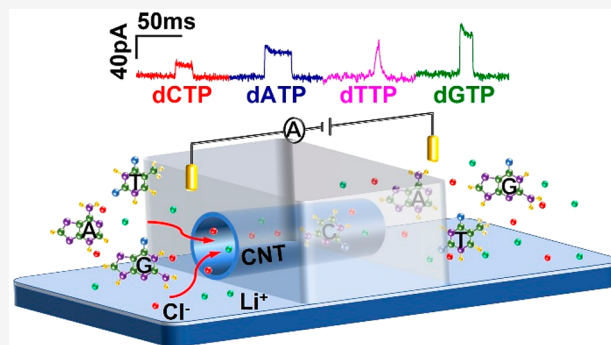
Metrics & More

Article Recommendations

Supporting Information

**ABSTRACT:** To be considered as a promising candidate for mimicking biological nanochannels, carbon nanotubes (CNTs) have been used to explore the mass transport phenomena in recent years. In this study, the single nucleotide transport phenomena are comparatively studied using individual CNTs with a length of  $\sim 15 \mu\text{m}$  and diameters ranging from 1.5 to 2.5 nm. In the case of CNTs with a diameter of 1.57–1.98 nm, the current traces of nucleotide transport are independent with the metallicity of CNTs and consist of single peak current pulses, whereas extraordinary stepwise current signals are observed in CNT with a diameter of 2.33 nm. It suggests that there is only one molecule in the nanochannel at a time until the diameter of CNT increases to 2.33 nm. Furthermore, it also demonstrates that the single nucleotides can be identified statistically according to their current pulses, indicating the potential application of CNT-based sensors for nucleotides identification.

**KEYWORDS:** Nanopore, Nanochannel, Carbon nanotube, Single nucleotides, Diameter dependence, Nucleotide transport



Biological nanochannels play an important role in various physiological processes. Facilitated by the significant advancements of nanotechnology, numerous artificial nanochannels have been fabricated to mimic the biological nanochannels.<sup>1–6</sup> Among them, carbon nanotubes (CNTs) have emerged as a competitive nanochannel due to the attractive advantages such as simple structure, uniform composition, large aspect ratio, and hydrophobic inner wall and can serve as a natural subfive-nanometer nanochannel without any special processing.<sup>6,7</sup>

For these features, many interesting and exceptional physical phenomena have been revealed, such as enhanced water transport<sup>8–11</sup> and ion mobility,<sup>12</sup> extreme phase transition temperatures of water,<sup>13</sup> ion selectivity,<sup>9,14,15</sup> power-law relation between ionic conductance and concentration,<sup>16–18</sup> and strong electroosmotic coupling.<sup>16</sup> In particular, the coherent resonance of ions in a  $\sim 500 \mu\text{m}$  long single-walled carbon nanotube (SWCNT) was observed by Strano's group.<sup>19–21</sup> However, the ions in the electrolyte might interfere with the analysis of other molecules in this system.

Compared with water and ions, the experimental studies involving biomolecular transport in CNT are rarely reported, and the results deviated from each other greatly. Lindsay's group reported the translocation of DNA oligomers through a  $2 \mu\text{m}$  long SWCNT.<sup>22,23</sup> Different from Strano et al.'s results, the electrolyte solution permits a steady current trace in their system, while DNA translocation produces electroosmotic

current pulses. After that, ultrashort SWCNT ( $\sim 10 \text{ nm}$ ) suspended in a planar lipid bilayer was utilized to detect modified 5-hydroxymethylcytosine in single-stranded DNA.<sup>12</sup> In contrast to the current-increasing pulses obtained by Lindsay's group, DNA translocation induces current blockages in this platform.

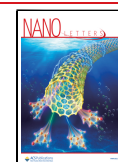
Upon the achievements concerning water and ions, most of the transport phenomena are strongly nanochannel diameter-dependent. Thus, it is reasonable to suspect that CNT diameter may affect DNA translocation. Furthermore, most studies on nucleotides distinguishment using solid-state nanopores focused on minimizing the interaction regions between nanopores and nucleotides,<sup>24–27</sup> it is still an unexplored territory to differentiate single nucleotides using CNT in a micrometer length.

Herein, the single nucleotides transport phenomena were studied comparatively using individual CNTs with a length of  $\sim 15 \mu\text{m}$  and diameters ranging from 1.5 to 2.5 nm. First, the kinetics of ion transport in CNT were investigated via scanning the time- and ion strength-dependent  $I$ - $V$  curves of CNTs.

**Received:** October 10, 2021

**Revised:** January 13, 2022

**Published:** January 18, 2022



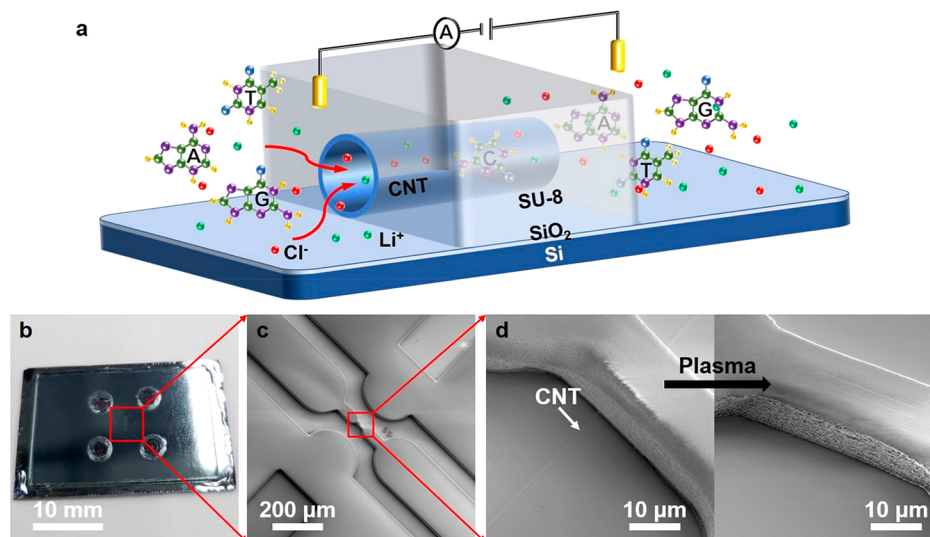


**Figure 1.** (a) Schematic diagram of single nucleotides transport through a CNT nanochannel. (b) The photograph of a CNT chip. (c) SEM image of the microchannels on the top of CNT. (d) SEM images of a CNT and the barrier on it before and after plasma treatment. The length of the barrier is about 12.56 μm.

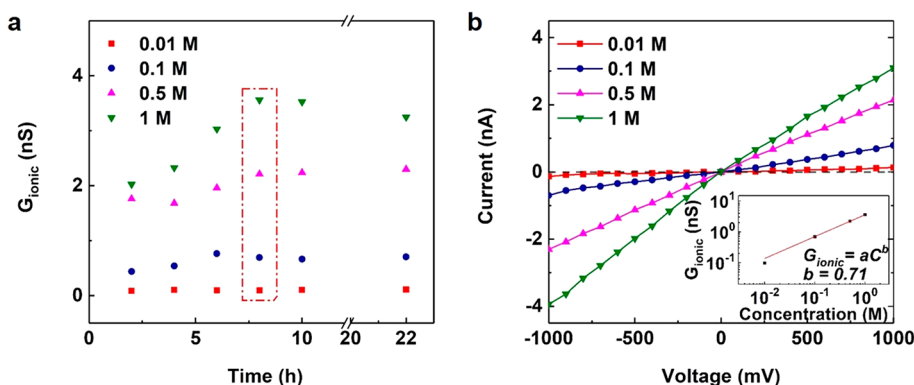


**Figure 2.** Time and concentration dependence of ion transport phenomena in SilkB7<sup>#</sup>. (a) The variations of ionic conductances in different concentrations of KCl buffers (buffered with 10 mM Tris and 1 mM EDTA at pH 8.0) over time. (b)  $I$ – $V$  curves of SilkB7<sup>#</sup> at KCl concentrations of 0.01, 0.1, 0.5, and 1 M after being immersed in a buffer for 8 h. Inset: The ionic conductance as a function of KCl concentration.

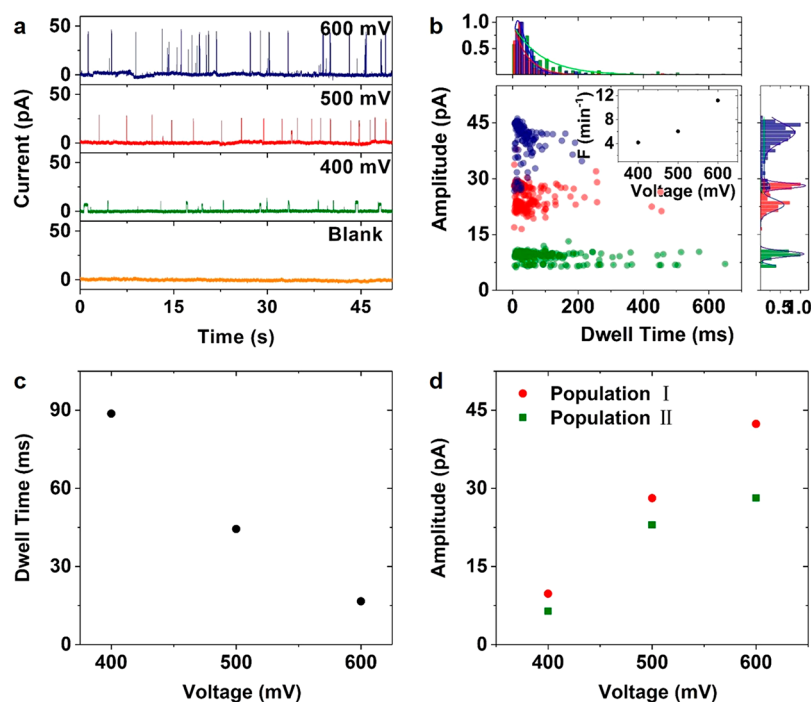
Whereafter, the dGTP transport was observed, and the current pulses derived from the electroosmotic effect were revealed associated with the CNT diameter and charged groups at the tubal ends. Finally, for all four types of nucleotides, we demonstrated the amplitudes and dwell times of the current pulses were strongly correlated to their properties in a 1.85 nm CNT. Results indicated the potential application of CNT-based sensors for nucleotides identification. Figure 1a exhibits the schematic diagram of single nucleotides transport through a CNT.

Figure 1b is a photograph of a CNT-based chip. The SEM images of the microchannels and barrier area before and after plasma treatment (Figure 1c,d) indicate there is only one open-ended CNT nanochannel under the barrier. No knotting and twisting are found from the fabricated portion of the CNTs (Figure S1a). The SEM images of all the barriers before and after plasma treatment and the AFM images of the CNTs and their corresponding profiles are shown in Figure S1b–c and Figure S2. The lengths of the barriers and the diameters of CNT are listed in Table S1.

## TIME AND CONCENTRATION DEPENDENCE OF ION TRANSPORT PHENOMENA IN CNT

In order to explore the ion transport and associated ionic equilibrium feature in CNTs, the time and concentration dependence on ionic conductance ( $G_{\text{ionic}}$ ) in SilkB7<sup>#</sup> were studied in KCl buffer. The initial  $G_{\text{ionic}}$  was measured after the introduction of buffer into microchannels for several minutes. Beyond our expectation, the  $I$ – $V$  curve characters are similar to that of open-circuit, indicating no ionic passage through CNT. It demonstrates the inner wall of the hydrophobic CNT is not wetted immediately by a buffer. Whereafter,  $G_{\text{ionic}}$  was measured with an interval of 2 h for a total of 22 h. The  $G_{\text{ionic}}$  of this CNT increases gradually with the increase in time and reaches equilibrium in 8 h at all buffer concentrations (Figure 2a), suggesting the wetting and ionic equilibrium in the CNT follows slow kinetics.

Since the ion mobility was reported to be enhanced in CNTs,<sup>9,17</sup> it rules out the possibility of the decrease in the ion diffusivity in such small channels. Bocquet et al. postulated that the inner surface of CNT is negatively charged due to the chemisorption of hydroxide.<sup>28</sup> Besides, all available cation sites of the negatively charged surfaces in nanochannel are reported



**Figure 3.** Voltage dependence of dGTP transport phenomena in SilkC8<sup>#</sup>. (a) Continuous 50 s characteristic current traces in the absence and presence of dGTP under different applied voltages. (b) Scatter plots of the amplitudes vs dwell times and corresponding normalized histograms. Inset: The dependence between event frequencies and applied voltages. (c) The dependence between dwell times and applied voltages. (d) The dependence between amplitudes and applied voltages. The red circles indicate the larger amplitudes (Population I), and the green squares indicate the smaller amplitudes (Population II). The experiments were performed with 1 M LiCl buffered with 10 mM Tris and 1 mM EDTA at pH 8.0. The concentration of dGTP was 100 pM. The applied voltages were +400, +500, and +600 mV, respectively. The diameter and length of the CNT were 1.57 nm and 16.17  $\mu\text{m}$ , respectively.

to be occupied first by protons, and their diffusivity is higher than other cations.<sup>29,30</sup> Thus, it takes a relatively long procedure to replace the protons for other cations, resulting in a time dependence on  $G_{\text{ionic}}$ .<sup>31</sup> On the other hand, although the rate of cation exchange is reported to be increased as the cation concentration increased,<sup>31</sup> the durations for equilibrium in our system seem almost the same under all concentrations, and the mechanism is unclear at present. The time dependence on  $G_{\text{ionic}}$  was also observed for SilkC8<sup>#</sup> in 1 M LiCl buffer. The  $G_{\text{ionic}}$  increases gradually with time elapsed and reaches the equilibrium in 10 h immersed into buffer (Figure S6a). A 2 h delay for equilibrium is likely a consequence of the smaller diameter of SilkC8<sup>#</sup>.

To further reveal the effect of ionic strength on ion transport properties in CNT, the  $I$ - $V$  curves of different concentrations at 8 h are compared in Figure 2b. The  $I$ - $V$  curves of SilkB7<sup>#</sup> show a primarily linear and slight asymmetric character under positive and negative voltages. Considering the structural and compositional uniformity of CNT, this may be due to the asymmetry of the anionic carboxylic groups on the rims of the plasma-treated CNT.<sup>23,32</sup> In contrast to SilkB7<sup>#</sup>, the  $I$ - $V$  curves of SilkC8<sup>#</sup> in 1 M LiCl buffer possess a good linear and symmetric relationship versus applied voltages (Figure S6b), which means the charge distribution on both tubal ends is symmetric. In addition, similar to the previous report, the change of  $G_{\text{ionic}}$  with buffer concentration follows a power function (Figure 2b, inset), revealing a strong coupling between water and ion transport in the nanochannel.<sup>16</sup> Moreover, the exponent is 0.707 in our case, slightly higher than 2/3, indicating the enhancement effect on electroosmotic coupling in our CNT system.<sup>18</sup>

### DIAMETER DEPENDENCE OF DGTP TRANSPORT PHENOMENA IN CNT

To clarify the role of diameter in nucleotide translocation, dGTP in four CNTs ( $d = 1.57, 1.85, 1.98,$  and  $2.33$  nm) was investigated. For SilkC8<sup>#</sup> ( $d = 1.57$  nm), the characteristic current traces in the absence and presence of dGTP in the electric field are represented in Figure 3a. Upon observation, the addition of dGTP to the *cis* channel produces coherent single peak current pulses. This observation indicates the translocation is actuated by electroosmotic flow rather than electrophoretic force, consistent with the phenomena observed by Lindsay's<sup>22,23</sup> and Chen's group.<sup>26</sup> Statistical scatter plots and corresponding histograms are shown in Figure 3b. The event frequency ( $F$ ) increases from 4.17 to 11.20/min with the increasing voltage from +400 to +600 mV (Figure 3b, inset). Furthermore, the dwell times are exponentially distributed with time constants of  $88.65 \pm 3.21, 44.37 \pm 3.01,$  and  $16.60 \pm 1.24$  ms at +400, +500, and +600 mV, respectively, which decreases linearly with the increase in applied voltage (Figure 3c). The increasing event frequency, as well as decreasing dwell time, indicates the signals are attributed to the translocation of dGTP through CNT.<sup>33</sup>

Unlike the single distribution of amplitudes in SilkD2<sup>#</sup> ( $d = 1.85$  nm) and SilkC5<sup>#</sup> ( $d = 1.98$  nm), dGTP generates two amplitude populations (both in Gaussian distribution) in the 1.57 nm CNT under all applied voltages (Figure 3b). Population I located at  $9.77 \pm 0.040, 28.11 \pm 0.064,$  and  $42.37 \pm 0.32$  pA, respectively, linearly increase with the elevation in applied voltage (Figure 3d, red). Meanwhile, Population II located at  $6.40 \pm 0.031, 22.95 \pm 0.18,$  and  $28.15 \pm 1.01$  pA, respectively, exhibiting a nonlinear dependence on

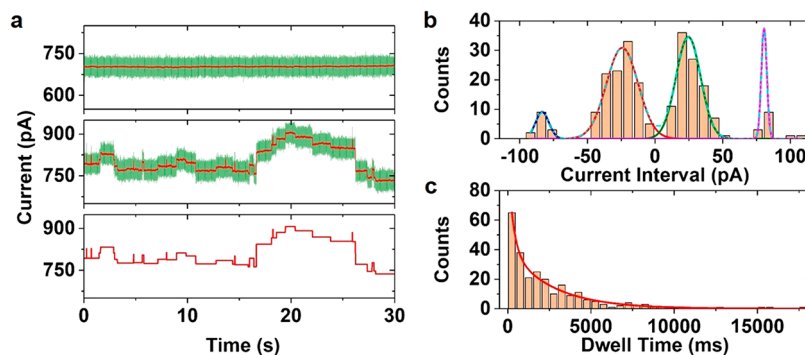


**Figure 4.** dGTP transport phenomenon in SilkD4<sup>#</sup>. (a) Continuous 30 s characteristic current traces in the absence (top) and presence (middle) of dGTP. The bottom panel: the mean currents of levels extracted from the middle panel. The green lines indicate the original current traces, and the red lines indicate the current traces filtered by a 200 Hz filter. (b) The histogram of current differences between two adjacent levels was extracted from 10 min of the current trace. (c) The histogram of dwell times of each single step level was extracted from 10 min of the current trace. The experiments were performed with 1 M LiCl buffered with 10 mM Tris and 1 mM EDTA at pH 8.0. The concentration of dGTP was 100 pM. The applied voltage was +400 mV. The diameter and length of the CNT were 2.33 nm and 15.85  $\mu\text{m}$ , respectively.

the applied voltage (Figure 3d, green). One plausible explanation for the generation of population II is that some counterions combined with the dGTP are stripped off due to the steric hindrance<sup>12</sup> and increased free-energy barrier for molecules entering into a small diameter CNT.<sup>34</sup>

The transport phenomena of dGTP in SilkC5<sup>#</sup> ( $d = 1.98$  nm) and SilkD2<sup>#</sup> ( $d = 1.85$  nm) were also analyzed. The current traces and the shape of characteristic pulses in the two CNTs are similar to that in SilkC8<sup>#</sup> (Figure S8a and Figure 5b). Figure S8a also displays that the event frequency increases sharply with the increase in applied voltage from +300 to +400 mV, suggesting the electric field force dominates the interactions between dGTP and CNT. The data show the average amplitudes in Gaussian fitting are  $74.86 \pm 0.092$  and  $116.77 \pm 0.25$  pA, while the most probable dwell times in exponential fitting are  $1576.40 \pm 229.02$  ms and  $1023.38 \pm 121.21$  ms, respectively (Figure S8b). Surprisingly, the interaction between dGTP and SilkC5<sup>#</sup> lasted for more than a second, much longer than that with other CNTs. Noticed that this CNT experienced longer plasma treatment, the extraordinary long dwell time might be attributed to the stronger interaction between dGTP and excess carboxyl groups at both ends of SilkC5<sup>#</sup>. Details of dGTP transport in SilkD2<sup>#</sup> will be discussed in the next section.

In CNTs with an inner diameter less than 2 nm, the transport phenomena of dGTP are similar to the ion transport reported by Strano's group.<sup>19,21</sup> Namely, there is only one molecule/ion in the nanochannel at a time, and the next molecule/ion gathered beside the mouth of CNT will enter the tube only after the existing molecule/ion emerges from the other side. Under this principle, the highly synchronized and rhythmic current signals are generated by dNTP/ion transport in CNT. Out of our expectation, the extraordinary stepwise current signals are observed in SilkD4<sup>#</sup> ( $d = 2.33$  nm) (Figure 4a, middle). The current trace in the absence of dGTP is shown in the top panel of Figure 4a for comparison. The bottom panel of Figure 4a shows the mean currents of levels extracted from the middle panel. Ten mins of the current trace were statistically analyzed for the distribution of the amplitudes and dwell times. The histogram of current differences between two adjacent levels is shown in Figure 4b, and the color lines indicate the Gaussian fit. The current increase (positive values) and decrease (negative values) are defined as the entrance and exit of dGTP(s), respectively. Interestingly, the peak values for

entrance and exit are almost symmetric, which locates at  $80.57 \pm 2.62$ ,  $24.58 \pm 0.95$ ,  $-24.21 \pm 1.21$ , and  $-83.38 \pm 3.18$  pA, respectively. According to the previous analyses from other CNTs, we presume the data distributed around  $24.58 \pm 0.95$  /  $-24.21 \pm 1.21$  pA signify the entrance/exit of one dGTP. The calculated probabilities for one molecule entrance and exit are  $\sim 88.25\%$ . Thus, the data distributed around  $80.57 \pm 2.62$  /  $-83.38 \pm 3.18$  pA indicate the entrance/exit of an aggregation of 3–4 dGTPs, and the probability for this situation is  $\sim 12\%$ . Considering the current trace is asymmetric, the molecules are supposed to experience a reaggregation in the nanochannel. Moreover, the event frequency of positive values (11.4/min) is very close to that of negative values (12.5/min) (Figure 4b), suggesting the opportunities for entrance and exit in these two states are almost the same. The statistical dwell times of each current level in exponential distribution are presented in Figure 4c, and the most probable dwell time is  $1564.02 \pm 125.56$  ms. In terms of metallicity dependence study, it is difficult to find a clue about the relationship between the CNT metallicity and DNA translocation according to the present analyses.

Since the signal-to-noise ratio of our CNT chips was comparatively low, a similar chip was fabricated with a quartzose substrate considering its lower capacitance.<sup>35</sup> Indeed, the current traces and the power spectral density (PSD) plots (Figure S9a–b) demonstrated the noise level was decreased significantly in quartzose chips compared to silicon-based CNT chips. Unfortunately, we did not observe any transport event through this CNT. Furthermore, it was hard to grow CNT with desired diameter and length on the quartzose substrate, which limited the current application. However, a novel transfer method could be used to obtain the desirable CNT on quartzose substrate.<sup>36</sup> In this case, the ideal chips with improved signal-to-noise are expected to be achieved based on this technology.

## NUCLEOTIDE-DEPENDENT TRANSPORT PHENOMENA IN CNT

Previously, the translocation events of dGTP have been reported in a 2  $\mu\text{m}$  long CNT by Lindsay's group.<sup>22</sup> However, the transport phenomena of other types of nucleotides in CNT are still unexplored territory. Therefore, the current traces of all four types of nucleotides in SilkD2<sup>#</sup>, a double-walled CNT with an inner diameter of 1.85 nm, were recorded to reveal the

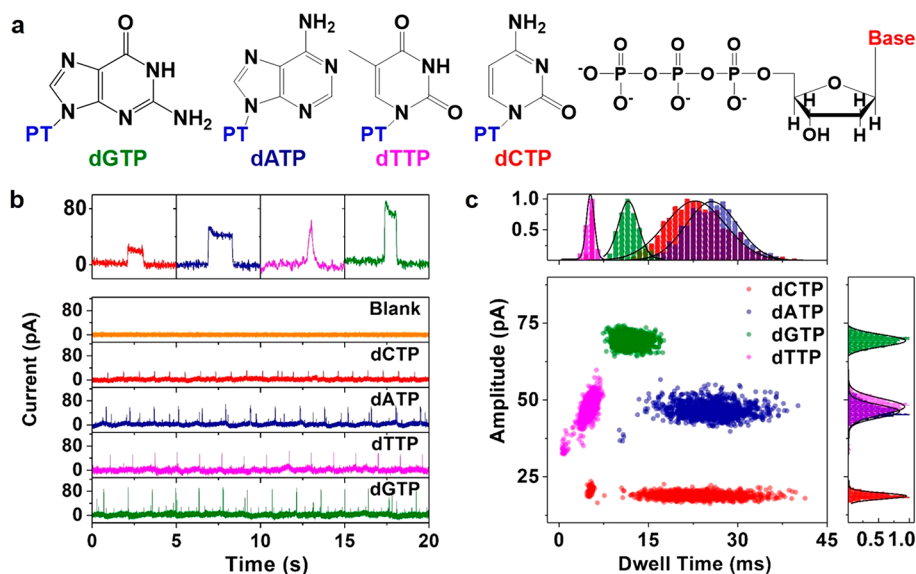


**Figure 5.** Molecular structures and translocation of dNTP in SilkD2<sup>#</sup>. (a) Molecular structures of bases and dNTP. (b) Characteristic current pulses of dNTPs (Top) and continuous 20 s characteristic current traces in the absence and presence of dNTPs (Bottom). (c) Scatter plots of the amplitudes vs dwell times and corresponding normalized histograms. The experiments were performed with 1 M LiCl buffered with 10 mM Tris and 1 mM EDTA at pH 8.0. The concentrations of dNTPs were 100 pM. The applied voltage was +400 mV. The diameter and length of the CNT were 1.85 nm and 12.56  $\mu\text{m}$ , respectively.

differences in their transport phenomena and explore the potential application of CNT-based sensors for nucleotides identification. The molecular structures of bases and deoxyribonucleotide triphosphate (dNTP) are illustrated in Figure 5a.

As illustrated in Figure 5b, all types of single nucleotides generate single peak current pulses under the applied voltage of +400 mV. Besides, the characteristic signals depend on the type of the single nucleotide (Figure 5b, top). The scatter plots of the four types of single nucleotides are distinguished, and the amplitudes of dGTP, dATP, dTTP, and dCTP are  $69.29 \pm 0.074$ ,  $47.79 \pm 0.056$ ,  $46.28 \pm 0.094$ , and  $18.70 \pm 0.065$  pA, respectively (Figure 5c), correlating with the volume of each nucleotide (G:  $359 \text{ \AA}^3$ ; A:  $349 \text{ \AA}^3$ ; T:  $339 \text{ \AA}^3$ ; C:  $324 \text{ \AA}^3$ ).<sup>37</sup> Nevertheless, the dwell time of dGTP, dATP, dTTP, and dCTP are  $11.62 \pm 0.084$ ,  $25.62 \pm 0.13$ ,  $5.23 \pm 0.031$ , and  $22.85 \pm 0.37$  ms, respectively, which are entirely irrelevant to their volume. In the 12.56  $\mu\text{m}$  CNT, the transport velocities of dGTP, dATP, dTTP, and dCTP are calculated to be 1082, 491, 2400, and 551 nm/ms, respectively, which are more than 2 orders of magnitude higher than those in MoS<sub>2</sub><sup>24</sup> and SiN<sub>x</sub> nanopores.<sup>26,27</sup> The enhanced rate agrees well with earlier studies for mass transport in CNTs, which could attribute to the frictionless slipping, large slip length, and confinement effect in hydrophobic nanochannels.<sup>8–12</sup> Note that the dwell time of dTTP is much shorter and that its distribution is narrower than other nucleotides. The difference appears to be attributed to the presence of the methyl group ( $-\text{CH}_3$ ) in dTTP, which increases the molecular hydrophobicity and decreases the interaction between dTTP and the hydrophilic groups ( $-\text{OH}$ ,  $-\text{COOH}$ , etc.) on CNT.<sup>38,39</sup> In contrast, the dwell time of dCTP, the other pyrimidine-based nucleotide, is much longer and with a broad distribution, which may arise from the complex interactions resulting from the small volume, electrostatic interactions, and hydrogen bonding.<sup>39</sup>

According to the average amplitude ( $I$ ) and the most probable dwell time ( $t$ ), the average number of charges ( $n$ )

contained in each spike can be deduced by  $n = I \times t/e$ , where  $e$  represents the elementary charge. As listed in Table S1, the number of charges for our CNTs ranges from  $10^6$  to  $10^8$ /spike, almost the same order of magnitude as the values obtained for dGTP<sup>22</sup> and 60 nt oligomer<sup>23</sup> ( $\sim 10^7$ /spike, Lindsay's group). Such enormous electroosmotic current cannot be simply attributed to the additional ions carried with the single nucleotide but is likely to arise from large changes in the concentration polarization outside the tubes.<sup>23,40</sup> Because of the indigent researches on the phenomenon, more theoretical and experimental investigations are desiderated to explore the underlying mechanisms.

It is a rather difficult and exciting experiment to fabricate the CNT chips. We only monitored stable current baseline in 6 out of 15 successfully fabricated chips combined with electronic force to drive nucleotides transport across these nanochannels. In our results, only 4 of them were observed the transport events. The ionic current of the 6 CNTs display no relationship with their diameters and metallicities (Table S1), and their giant ionic currents are likely a consequence of the nearly frictionless flow of water inside the CNTs.<sup>41</sup>

Furthermore, SilkD2<sup>#</sup> was the only chip in which the current traces of all four types of nucleotides were recorded. One reason is that SilkD2<sup>#</sup> was the only survivor without leaking issue after many times of rinse. On the other hand, it may be due to the unique character of each CNT, which makes the transport phenomena observed in our experiment relatively CNT individual-independent. This problem should be avoided if chips are fabricated by different portions of the same CNT.<sup>42</sup> Indeed, many obstacles are waiting to conquer (i.e., the robustness of the chip), and we would like to share our available results with the researchers working in this field, which may accelerate the pace to touch the fascinating application in the nanofluidics regime.

In conclusion, CNT-based nanochannels were fabricated using standard photolithography. The time and concentration dependence of ion transport in CNTs were studied by

investigating the variation of  $G_{\text{ionic}}$  and the shape of  $I-V$  curves. Results demonstrate that the inner surface of CNT is negatively charged, resulting in slow kinetics of ionic equilibrium in the nanochannel. Meanwhile, the electro-osmotic coupling effect was enhanced in CNT, leading to a power-law relation between the ionic conductance and electrolyte concentration, with a power exponent close to 2/3. Furthermore, the diameter dependence of dGTP transport in CNTs was observed. For narrow CNTs, single peak current pulses were the only component of the current traces. It was hypothesized there is only one nucleotide in the nanochannel at a time. In particular, based on the stepwise current levels extracted from the current trace of a 2.33 nm CNT, multiple nucleotides may exist in the CNT nanochannel at the same time, and there is a probability of  $\sim 12\%$  for the entrance of aggregated dGTPs. Finally, four types of single nucleotides can be identified according to the nucleotide-dependent current pulses through the same CNT. It is expected to elucidate the underlying mechanism accounting for these phenomena based on both experimental and theoretical investigations.

## ■ ASSOCIATED CONTENT

### SI Supporting Information

The Supporting Information is available free of charge at <https://pubs.acs.org/doi/10.1021/acs.nanolett.1c03910>.

Materials and methods; length, diameter, metallicity, plasma treatment, the average number of charges in each spike, and ionic current of the as-prepared CNTs; schematic diagrams of the fabrication process to fabricate CNT devices; SEM images of the as-prepared CNTs, the exposed CNTs, and barriers before and after plasma treatment; AFM images of the as-prepared CNTs and their corresponding profiles; Raman spectra of the as-prepared CNTs; plasma treatment effect; time dependence of ion transport phenomena in SilkC8<sup>#</sup>;  $I-V$  curves of control devices; voltage dependence of dGTP transport phenomena in SilkC5<sup>#</sup> (PDF)

## ■ AUTHOR INFORMATION

### Corresponding Authors

**Jiahu Yuan** – Chongqing Institute of Green and Intelligent Technology, Chinese Academy of Sciences, Chongqing 400714, China; Chongqing School, University of Chinese Academy of Sciences, Chongqing 400714, China; Phone: +86-23-6593-5063; Email: [yjh@cigit.ac.cn](mailto:yjh@cigit.ac.cn)

**Jin Zhang** – Beijing Science and Engineering Center for Nanocarbons, School of Materials Science and Engineering, College of Chemistry and Molecular Engineering, Peking University, Beijing 100871, China; [orcid.org/0000-0003-3731-8859](https://orcid.org/0000-0003-3731-8859); Phone: +86-10-6275-2555; Email: [jinzhang@pku.edu.cn](mailto:jinzhang@pku.edu.cn)

**Deqiang Wang** – Chongqing Institute of Green and Intelligent Technology, Chinese Academy of Sciences, Chongqing 400714, China; Chongqing School, University of Chinese Academy of Sciences, Chongqing 400714, China; [orcid.org/0000-0002-3151-6769](https://orcid.org/0000-0002-3151-6769); Phone: +86-23-6593-5063; Email: [dqwang@cigit.ac.cn](mailto:dqwang@cigit.ac.cn)

### Authors

**Yunjiao Wang** – Chongqing Institute of Green and Intelligent Technology, Chinese Academy of Sciences, Chongqing 400714, China; Chongqing School, University of Chinese

Academy of Sciences, Chongqing 400714, China;

[orcid.org/0000-0002-7002-0889](https://orcid.org/0000-0002-7002-0889)

**Zequn Wang** – Beijing Science and Engineering Center for Nanocarbons, School of Materials Science and Engineering, College of Chemistry and Molecular Engineering, Peking University, Beijing 100871, China

**Liang Wang** – Chongqing Institute of Green and Intelligent Technology, Chinese Academy of Sciences, Chongqing 400714, China; Chongqing School, University of Chinese Academy of Sciences, Chongqing 400714, China; Chongqing Key Laboratory of Intelligent Medicine Engineering for Hepatopancreatobiliary Diseases, Chongqing 401147, China; [orcid.org/0000-0002-7404-4319](https://orcid.org/0000-0002-7404-4319)

**Tianze Tong** – Beijing Science and Engineering Center for Nanocarbons, School of Materials Science and Engineering, College of Chemistry and Molecular Engineering, Peking University, Beijing 100871, China

**Xiaoling Zhang** – Chongqing Institute of Green and Intelligent Technology, Chinese Academy of Sciences, Chongqing 400714, China; Chongqing School, University of Chinese Academy of Sciences, Chongqing 400714, China

**Shaoyi Fang** – Chongqing Institute of Green and Intelligent Technology, Chinese Academy of Sciences, Chongqing 400714, China; Chongqing School, University of Chinese Academy of Sciences, Chongqing 400714, China

**Wanyi Xie** – Chongqing Institute of Green and Intelligent Technology, Chinese Academy of Sciences, Chongqing 400714, China; Chongqing School, University of Chinese Academy of Sciences, Chongqing 400714, China

**Liyuan Liang** – Chongqing Institute of Green and Intelligent Technology, Chinese Academy of Sciences, Chongqing 400714, China; Chongqing School, University of Chinese Academy of Sciences, Chongqing 400714, China;

[orcid.org/0000-0003-3990-064X](https://orcid.org/0000-0003-3990-064X)

**Bohua Yin** – Chongqing Institute of Green and Intelligent Technology, Chinese Academy of Sciences, Chongqing 400714, China; Chongqing School, University of Chinese Academy of Sciences, Chongqing 400714, China

Complete contact information is available at:

<https://pubs.acs.org/doi/10.1021/acs.nanolett.1c03910>

### Author Contributions

The authors contributed to the following: Y.W., methodology, investigation, formal analysis, data curation, visualization, and original draft writing; Z.W. and T.T., methodology, investigation, and formal analysis; L.W., methodology, formal analysis, and funding acquisition; X.Z., S.F., W.X., and B.Y., investigation, software, and formal analysis; L.L., formal analysis and funding acquisition; J.Y. and J.Z., supervision and project administration; D.W., conceptualization, methodology, supervision, project administration, and writing, reviewing, and editing. All authors have approved the final version of the manuscript.

### Funding

This project was financially supported by the National Natural Science Foundation of China (31800711), Chongqing Talents: Exceptional Young Talents Project (CQYC201905007, cstc2021ycjh-bgzxm0016), the Natural Science Foundation of Chongqing (cstc2021jcyj-bshX0160), and the Excellent Youth Foundation of Chongqing Scientific Committee (cstc2021jcyj-jq0030). We would also like to thank the support from Pioneer Hundred Talents Program (to L.W.),

the Youth Innovation Promotion Association (to Y.W.), West Light Foundation (to L.L.) of the Chinese Academy of Sciences, and the University of Chinese Academy of Sciences.

## Notes

The authors declare no competing financial interest.

## ACKNOWLEDGMENTS

We sincerely thank Dr. Bin Mu (Lanzhou Institute of Chemical Physics, Chinese Academy of Sciences, China) and Dr. Qiang Zhao (Chongqing University, China) for their contribution and discussion to this work. We also would like to thank the University of Chinese Academy of Sciences.

## REFERENCES

- (1) Drndić, M. 20 years of solid-state nanopores. *Nature Reviews Physics* **2021**, *3*, 606.
- (2) Fan, R.; Karnik, R.; Yue, M.; Li, D.; Majumdar, A.; Yang, P. DNA translocation in inorganic nanotubes. *Nano Lett.* **2005**, *5* (9), 1633–1637.
- (3) Liu, Y.; Yobas, L. Slowing DNA translocation in a nanofluidic field-effect transistor. *ACS Nano* **2016**, *10* (4), 3985–3994.
- (4) Zhang, P.; Xia, M.; Zhuge, F.; Zhou, Y.; Wang, Z.; Dong, B.; Fu, Y.; Yang, K.; Li, Y.; He, Y.; Scheicher, R. H.; Miao, X. S. Nanochannel-based transport in an interfacial memristor can emulate the analog weight modulation of synapses. *Nano Lett.* **2019**, *19* (7), 4279–4286.
- (5) Siria, A.; Poncharal, P.; Bianco, A.-L.; Fulcrand, R.; Blase, X.; Purcell, S. T.; Bocquet, L. Giant osmotic energy conversion measured in a single transmembrane boron nitride nanotube. *Nature* **2013**, *494* (7438), 455–458.
- (6) Guo, S.; Meshot, E. R.; Kuykendall, T.; Cabrini, S.; Fornasiero, F. Nanofluidic transport through isolated carbon nanotube channels: Advances, controversies, and challenges. *Adv. Mater.* **2015**, *27* (38), 5726–5737.
- (7) Guo, J.; He, J.; Zeng, B. Carbon Nanotube Based Nanopore and Nanofluidic Devices Towards Sensing Applications. *Current Nanoscience* **2016**, *12* (4), 421–428.
- (8) Holt, J. K.; Park, H. G.; Wang, Y.; Stadermann, M.; Artyukhin, A. B.; Grigoropoulos, C. P.; Noy, A.; Bakajin, O. Fast mass transport through sub-2-nanometer carbon nanotubes. *Science* **2006**, *312* (5776), 1034–1037.
- (9) Tunuguntla, R. H.; Henley, R. Y.; Yao, Y.-C.; Pham, T. A.; Wanunu, M.; Noy, A. Enhanced water permeability and tunable ion selectivity in subnanometer carbon nanotube porins. *Science* **2017**, *357* (6353), 792–796.
- (10) Secchi, E.; Marbach, S.; Niguès, A.; Stein, D.; Siria, A.; Bocquet, L. Massive radius-dependent flow slippage in carbon nanotubes. *Nature* **2016**, *537* (7619), 210–213.
- (11) Falk, K.; Sedlmeier, F.; Joly, L.; Netz, R. R.; Bocquet, L. Molecular origin of fast water transport in carbon nanotube membranes: superlubricity versus curvature dependent friction. *Nano Lett.* **2010**, *10* (10), 4067–4073.
- (12) Liu, L.; Yang, C.; Zhao, K.; Li, J.; Wu, H. Ultrashort single-walled carbon nanotubes in a lipid bilayer as a new nanopore sensor. *Nat. Commun.* **2013**, *4*, 2989.
- (13) Agrawal, K. V.; Shimizu, S.; Drahusshuk, L. W.; Kilcoyne, D.; Strano, M. S. Observation of extreme phase transition temperatures of water confined inside isolated carbon nanotubes. *Nat. Nanotechnol.* **2017**, *12* (3), 267–273.
- (14) Fornasiero, F.; Park, H. G.; Holt, J. K.; Stadermann, M.; Grigoropoulos, C. P.; Noy, A.; Bakajin, O. Ion exclusion by sub-2-nm carbon nanotube pores. *Proc. Natl. Acad. Sci. U. S. A.* **2008**, *105* (45), 17250–17255.
- (15) Li, Z.; Li, Y.; Yao, Y.-C.; Aydin, F.; Zhan, C.; Chen, Y.; Elimelech, M.; Pham, T. A.; Noy, A. Strong Differential Monovalent Anion Selectivity in Narrow Diameter Carbon Nanotube Porins. *ACS Nano* **2020**, *14* (5), 6269–6275.
- (16) Yao, Y.-C.; Taqieddin, A.; Alibakhshi, M. A.; Wanunu, M.; Aluru, N. R.; Noy, A. Strong Electroosmotic Coupling Dominates Ion Conductance of 1.5 nm Diameter Carbon Nanotube Porins. *ACS Nano* **2019**, *13* (11), 12851–12859.
- (17) Secchi, E.; Niguès, A.; Jubin, L.; Siria, A.; Bocquet, L. Scaling behavior for ionic transport and its fluctuations in individual carbon nanotubes. *Phys. Rev. Lett.* **2016**, *116* (15), 154501.
- (18) Manghi, M.; Palmeri, J.; Yazda, K.; Henn, F.; Jourdain, V. Role of charge regulation and flow slip in the ionic conductance of nanopores: An analytical approach. *Phys. Rev. E* **2018**, *98* (1), 012605.
- (19) Lee, C. Y.; Choi, W.; Han, J.-H.; Strano, M. S. Coherence resonance in a single-walled carbon nanotube ion channel. *Science* **2010**, *329* (5997), 1320–1324.
- (20) Choi, W.; Lee, C. Y.; Ham, M.-H.; Shimizu, S.; Strano, M. S. Dynamics of simultaneous, single ion transport through two single-walled carbon nanotubes: observation of a three-state system. *J. Am. Chem. Soc.* **2011**, *133* (2), 203–205.
- (21) Choi, W.; Ulissi, Z. W.; Shimizu, S. F.; Bellisario, D. O.; Ellison, M. D.; Strano, M. S. Diameter-dependent ion transport through the interior of isolated single-walled carbon nanotubes. *Nat. Commun.* **2013**, *4* (1), 1–8.
- (22) He, J.; Liu, H.; Pang, P.; Cao, D.; Lindsay, S. Translocation events in a single-walled carbon nanotube. *J. Phys.: Condens. Matter* **2010**, *22* (45), 454112.
- (23) Liu, H.; He, J.; Tang, J.; Liu, H.; Pang, P.; Cao, D.; Krstic, P.; Joseph, S.; Lindsay, S.; Nuckolls, C. Translocation of single-stranded DNA through single-walled carbon nanotubes. *Science* **2010**, *327* (5961), 64–67.
- (24) Feng, J.; Liu, K.; Bulushev, R. D.; Khlybov, S.; Dumcenco, D.; Kis, A.; Radenovic, A. Identification of single nucleotides in MoS<sub>2</sub> nanopores. *Nat. Nanotechnol.* **2015**, *10* (12), 1070–1076.
- (25) Tsutsui, M.; Taniguchi, M.; Yokota, K.; Kawai, T. Identifying single nucleotides by tunnelling current. *Nat. Nanotechnol.* **2010**, *5* (4), 286–290.
- (26) Yang, H.; Li, Z.; Si, W.; Lin, K.; Ma, J.; Li, K.; Sun, L.; Sha, J.; Chen, Y. Identification of single nucleotides by a tiny charged solid-state nanopore. *J. Phys. Chem. B* **2018**, *122* (32), 7929–7935.
- (27) Goto, Y.; Matsui, K.; Yanagi, I.; Takeda, K.-i. Silicon nitride nanopore created by dielectric breakdown with a divalent cation: deceleration of translocation speed and identification of single nucleotides. *Nanoscale* **2019**, *11* (30), 14426–14433.
- (28) Grosjean, B.; Pean, C.; Siria, A.; Bocquet, L.; Vuilleumier, R.; Bocquet, M.-L. Chemisorption of hydroxide on 2D materials from DFT calculations: graphene versus hexagonal boron nitride. *J. Phys. Chem. Lett.* **2016**, *7* (22), 4695–4700.
- (29) Raider, S.; Gregor, L.; Flitsch, R. Transfer of Mobile Ions from Aqueous Solutions to the Silicon Dioxide Surface. *J. Electrochem. Soc.* **1973**, *120* (3), 425–431.
- (30) Tunuguntla, R.; Allen, F.; Kim, K.; Belliveau, A.; Noy, A. Ultra-Fast Proton Transport in Sub-1-nm Diameter Carbon Nanotube Porins. *Biophys. J.* **2016**, *110* (3), 338a.
- (31) Duan, C.; Majumdar, A. Anomalous ion transport in 2-nm hydrophilic nanochannels. *Nat. Nanotechnol.* **2010**, *5* (12), 848–852.
- (32) Ying, C.; Zhang, Y.; Feng, Y.; Zhou, D.; Wang, D.; Xiang, Y.; Zhou, W.; Chen, Y.; Du, C.; Tian, J. 3D nanopore shape control by current-stimulus dielectric breakdown. *Appl. Phys. Lett.* **2016**, *109* (6), 063105.
- (33) Wang, Y.; Cheng, M.; Wang, L.; Zhou, D.; He, S.; Liang, L.; Zhang, F.; Liu, C.; Wang, D.; Yuan, J. Nanocrystalline graphite nanopores for DNA sensing. *Carbon* **2021**, *176*, 271–278.
- (34) Peter, C.; Hummer, G. Ion transport through membrane-spanning nanopores studied by molecular dynamics simulations and continuum electrostatics calculations. *Biophys. J.* **2005**, *89* (4), 2222–2234.
- (35) Pitchford, W. H.; Kim, H.-J.; Ivanov, A. P.; Kim, H.-M.; Yu, J.-S.; Leatherbarrow, R. J.; Albrecht, T.; Kim, K.-B.; Edel, J. B. Synchronized optical and electronic detection of biomolecules using a low noise nanopore platform. *ACS Nano* **2015**, *9* (2), 1740–1748.

(36) Song, W.; Pang, P.; He, J.; Lindsay, S. Optical and electrical detection of single-molecule translocation through carbon nanotubes. *ACS Nano* **2013**, *7* (1), 689–694.

(37) Zwolak, M.; Di Ventra, M. Colloquium: Physical approaches to DNA sequencing and detection. *Rev. Mod. Phys.* **2008**, *80* (1), 141–165.

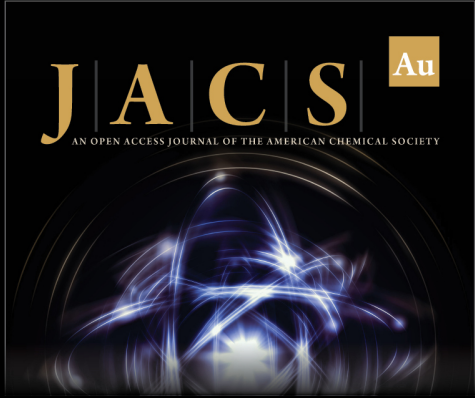
(38) Clarke, J.; Wu, H.-C.; Jayasinghe, L.; Patel, A.; Reid, S.; Bayley, H. Continuous base identification for single-molecule nanopore DNA sequencing. *Nat. Nanotechnol.* **2009**, *4* (4), 265–270.

(39) Jeong, K.-B.; Luo, K.; Lee, H.; Lim, M.-C.; Yu, J.; Choi, S.-J.; Kim, K.-B.; Jeon, T.-J.; Kim, Y.-R. Alpha-Hederin Nanopore for Single Nucleotide Discrimination. *ACS Nano* **2019**, *13* (2), 1719–1727.


(40) Jin, X.; Joseph, S.; Gatimu, E. N.; Bohn, P. W.; Aluru, N. R. Induced electrokinetic transport in micro- nanofluidic interconnect devices. *Langmuir* **2007**, *23* (26), 13209–13222.


(41) Pang, P.; He, J.; Park, J. H.; Krstić, P. S.; Lindsay, S. Origin of giant ionic currents in carbon nanotube channels. *ACS Nano* **2011**, *5* (9), 7277–7283.


(42) Zhu, Z.; Wei, N.; Cheng, W.; Shen, B.; Sun, S.; Gao, J.; Wen, Q.; Zhang, R.; Xu, J.; Wang, Y.; Wei, F. Rate-selected growth of ultrapure semiconducting carbon nanotube arrays. *Nat. Commun.* **2019**, *10* (1), 4467.



**JACS** Au  
AN OPEN ACCESS JOURNAL OF THE AMERICAN CHEMICAL SOCIETY

 Editor-in-Chief  
**Prof. Christopher W. Jones**  
Georgia Institute of Technology, USA

**Open for Submissions** 

pubs.acs.org/jacsau  ACS Publications  
Most Trusted. Most Cited. Most Read.